Additive Manufacturing: Metallurgy, Cut Analysis & Porosity

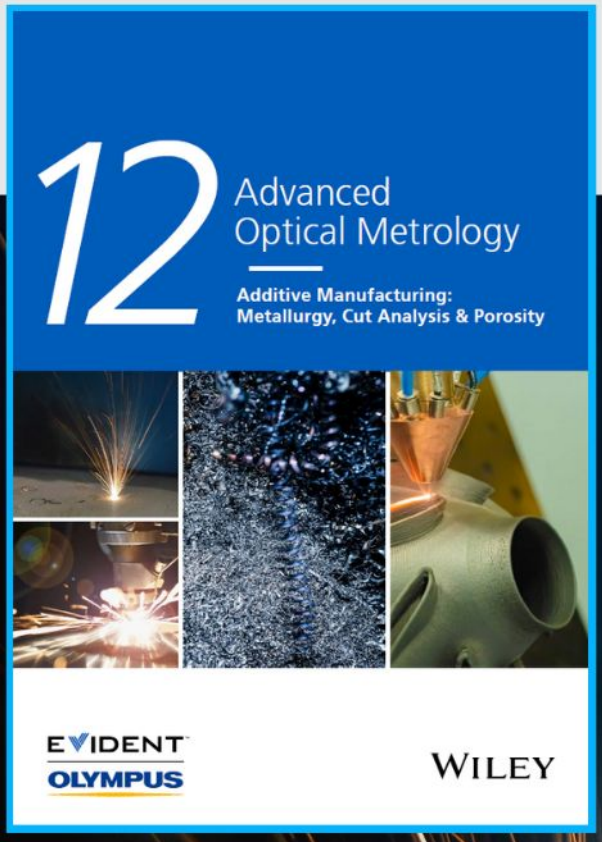

The latest eBook from Advanced Optical Metrology. Download for free.

In industry, sector after sector is moving away from conventional production methods to additive manufacturing, a technology that has been recommended for substantial research investment.

Download the latest eBook to read about the applications, trends, opportunities, and challenges around this process, and how it has been adapted to different industrial sectors.

EVIDENT
OLYMPUS

WILEY

NANO · MICRO small
www.small-journal.com

Supramolecular Network Structured Gel Polymer Electrolyte with High Ionic Conductivity for Lithium Metal Batteries

Fei Chen, Changxiang Guo, Honghao Zhou, Muhammad Wakil Shahzad, Terence Xiaoteng Liu, Sokolskyi Oleksandr, Jining Sun, Sheng Dai, and Ben Bin Xu**

Polymer-based solid electrolytes (PSEs) offer great promise in developing lithium metal batteries due to their attractive features such as safety, light weight, low cost, and high processability. However, a PSE-based lithium battery usually requires a relatively high temperature (60 °C or above) to complete charge and discharge due to the poor ionic conductivity of PSEs. Herein, a gel polymer electrolytes (GPEs) film with a supramolecular network structure through a facile one-step photopolymerization is designed and developed. The crosslinked structure and quadruple hydrogen bonding fulfil the GPEs with high thermal stability and good mechanical property with a maximum tensile strain of 48%. The obtained GPEs possess a high ionic conductivity of 3.8×10^{-3} S cm^{-1} at 25 °C and a decomposition voltage ≥ 4.6 V (vs Li/Li$^+$). The cells assembled with $LiFePO_4$ cathode and Li anode, present an initial discharge specific capacity of 155.6 mAh g^{-1} and a good cycling efficiency with a capacity retention rate of 81.1% after 100 charges/discharge cycles at 0.1 C at ambient temperature. This work encompasses a route to develop high performance PSEs that can be operated at room temperature for future lithium metal batteries.

1. Introduction

Operational safety has drawn considerable attention for lithium-ion (Li-ion) batteries, where the replacement of flammable liquid electrolytes with solid electrolytes appears to be a sensible choice.[1] Besides, the solid-state electrolyte is featured for higher energy density to benefit future Li-ion batteries.[2] Lithium metal anode (3860 mAh g^{-1}) has a higher theoretical specific capacity and lower electrochemical potential (−3.04 V vs hydrogen potential) than graphite anode (372 mAh g^{-1}), and replacing graphite anode (250 Wh Kg^{-1}) with lithium metal anode (440 Wh Kg^{-1}) can double the effective energy for battery.[3] However, the lithium dendrite on the anode can trigger the diaphragm to fracture during the operation, the resulting short-circuit in battery ultimately lead to fire and losses of life or property.[4] The replacement of diaphragm by solid-state electrolytes dramatically simplifies the battery production process and greatly enhances the safety. Polymer-based solid-state electrolytes (PSEs) has emerged to lead solid-state electrolyte technology for its simple production, molecular modifiability, low cost, and good processability.[5] However, the low ionic conductivity of PSEs seriously hinders their applications.[6]

To increase the ionic conductivity of PSEs, researchers have made a variety of attempts, for example, replacing lithium salts with different anions, adding plasticizers, preparing composite polymer electrolytes, etc. Polyethylene oxide (PEO) has been known as a promising candidate for PSEs, for its unique capability to dissolve lithium ions. But the high crystallinity of PEO at room temperature leads to a low ionic conductivity (10^{-8}≈10^{-5} S cm^{-1}), therefore its actual operating temperature needs to be 60 °C or above.[7] Notably, Wang and co-workers have managed to increase the ionic conductivity of polymer electrolyte to 1.1×10^{-4} S cm^{-1} at 35 °C by reducing the crystallinity of PEO and the Li/PEO-HPMA/$LiFePO_4$ (LFP) cell can maintain a reversible capacity of 80.4 mAh g^{-1} at 1C rate.[8] Wan et al. mixed PEO and $Li_7La_3Zr_2O_{12}$ to produce a composite solid-state electrolyte film with improved ionic conductivity to obtain specific capacity 158.7 mAh g^{-1} at 0.1 C in LFP/PLLN/Li batteries, with an operational temperature below 45 °C.[9] Bouchet and co-workers prepared a single-ion conductor triblock copolymer P(STFSILi)-*b*-PEO-*b*-P(STFSILi) based LFP/Li with a discharge specific capacity

F. Chen, C. Guo
Shaanxi Key Laboratory of Energy Chemical Process Intensification
School of Chemical Engineering and Technology
Xi'an Jiaotong University
Xi'an, Shaanxi 710049, P. R. China
E-mail: feichen@xjtu.edu.cn
H. Zhou, M. Shahzad, T. Liu, B. Xu
Mechanical and Construction Engineering
Faculty of Engineering and Environment
Northumbria University
Newcastle upon Tyne NE1 8ST, UK
E-mail: ben.xu@northumbria.ac.uk
S. Oleksandr
Department of Chemical
Polymer and Silicate Engineering
Igor Sikorsky Kyiv Polytechnic Institute
03056, Kyiv, Ukraine
J. Sun
School of Mechanical Engineering
Dalian University of Technology
Dalian 116024, China
S. Dai
School of Chemical and Process Engineering
University of Leeds
Leeds LS2 9JT, UK
The ORCID identification number(s) for the author(s) of this article can be found under https://doi.org/10.1002/smll.202106352.

DOI: 10.1002/smll.202106352

of 160 mAh g^{-1} at C/8 under 80 °C.[10] Feng and co-workers developed a single Li-ion polymer electrolyte approach with utilizing P(SSPSILi-*alt*-MA) as the active ingredient and realized single LFP/Li battery with a specific capacity higher than 150 mAh g^{-1} at 0.02C under 80 °C.[11] Xue et al. synthesized a cross-linked polymer solid-state electrolyte, CPSHPE, with a good flame retardancy, self-healing capability and an initial discharge capacity of 130 mAh g^{-1} at 0.1C below 60 °C with LFP/Li cells.[12] Although ionic conductivity can be significantly enhanced using above approaches, high operational temperature of charge/discharge cycles still remains as a challenge in exploring solid-state electrolyte applications in lithium metal batteries.

Gel polymer electrolyte (GPE), a supramolecular network structured polymer electrolyte, hold more potentials for commercialization than other PSEs, with high ionic conductivity and superior electrode/electrolyte interfacial properties, excellent mechanical properties (strength, flexibility, etc.), and enhanced safety. Cross-linked polymers offer many advantages in achieving mechanically robust polymer electrolyte, including easy synthesis, the ability to suppress the crystallinity of polymer, and increased polymer mechanical strength.[13] Here, we propose a supramolecular network structured polymer electrolyte approach to achieve good mechanical properties and high ionic conductivity electrolytes. The poly(ethylene glycol) methyl ether methacrylate (PEGMA), 2-(3-(6-methyl-4-oxo-1,4-dihydropyrimidin-2-yl) ureido)ethyl methacrylate (UPyMA), tripropylene glycol diacrylate (TPGDA), and 1-Allyl-3-methylimidazolium Bis(trifluoromethanesulfonyl)imide (AMIMTFSI) will form the skeleton of polymer electrolyte, with UPyMA in the cross-linked structure to provide better mechanical strength since their dimers will form a quadruple hydrogen bonding interaction. The supramolecular gel network also contains small residual molecules such as ionic liquid (IL) monomers and prepolymers that have not undergone polymerization, thus providing a high ionic conductivity. Furthermore, the GPEs developed in this paper have been assembled in lithium metal batteries and have been tested with good charge/discharge cycle capability at room temperature (25 °C).

2. Results and Discussion

2.1. Design and Preparation of PUTP Electrolytes

The supramolecular network structured gel is photosynthesized (**Figure 1**). In the supramolecular network structure, PEGMA and AMIMTFSI not only provide the polymeric substrate but also effectively influence the transport of ions. Meanwhile, the quadruple hydrogen bonding networks constructed by the interaction of UPyMA dimers give the polymer electrolyte good mechanical performance. **Table 1** shows the monomers proportions, the glass transition temperature and ionic conductivity of PUTP GPE samples.

Fourier-transform infrared spectra (FTIR) were employed to verify the polymerization of monomers. The FTIR spectra clearly show the chemical structure of UPyMA, PEGMA, TPGDA, AMIMTFSI, PUTP1, PUTP2, and PUTP3 (Figures S1–S7, Supporting Information). For the monomers of AMIMTFSI, UPyMA, the characteristic peaks stretching bands of C=C at 1650 cm^{-1}. PEGMA and TPGDA, the stretching bands of C=C and C=O give their characteristic peaks at 1638 and 1726 cm^{-1}. After polymerization, the C=C stretching vibrations no disappear in PUTP1, PUTP2, and PUTP3 samples, demonstrating that the polymerization is not fully completed under the initiation of UV light. These monomers or prepolymers, which do not polymerize, are existing in the supramolecular network in a free form, thus forming ion transport channels with the PEG/poly(ionic liquid) chains in the crosslinked network. For the PUTP, four characteristic absorption peaks of the TFSI anion can be observed in the spectrum at 1060, 1138, 1196, and 1350 cm^{-1}, indicating that the TFSI is successfully dispersed in the network.

The PUTP electrolyte system contains a cross-linked supramolecular network formed by TPGDA as a cross-linking agent and UPyMA quadruple hydrogen bonding. **Figure 2**a shows the optical photographs for PUTP1, PUTP2, and PUTP3 samples, respectively. The elasticity (flexibility) of solid electrolyte is demonstrated by folding PUTP1 in a different direction (Figure 2b,c), where the film can be folded and do not break. The flexible nature of polymeric solid electrolytes offers a great advantage to be applied in flexible electronic devices.

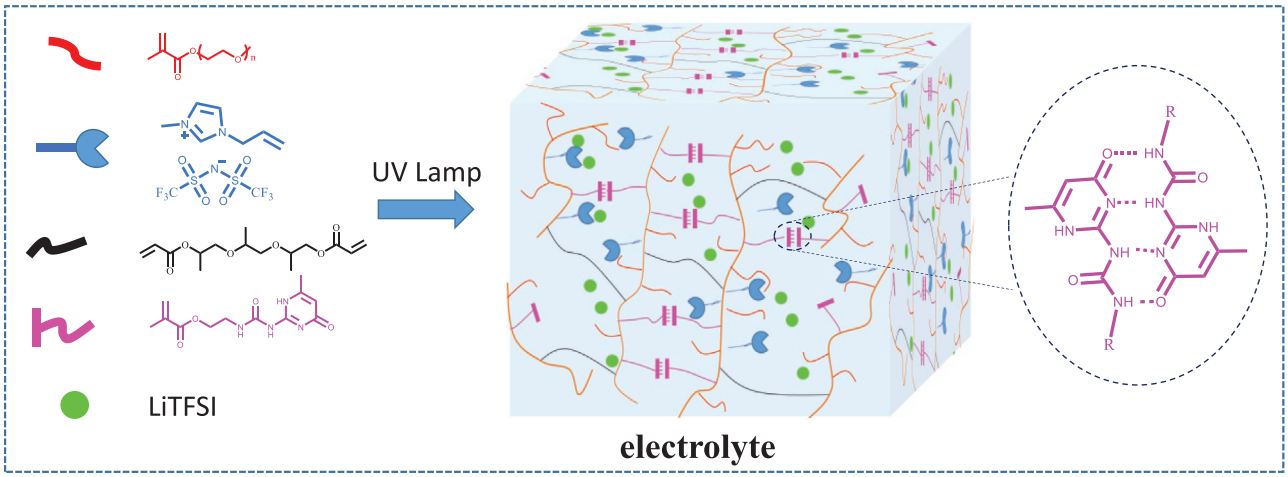

Figure 1. Schematic illustration of the monomers and one-step photosynthesis of PUTP GPEs.

Table 1. Molar ratio of PEGMA to UPyMA, T_g and ionic conductivity of PUTP electrolyte.

Electrolyte	PEGMA:UPyMA (by mole)	T_g [°C]	σ at 25 [°C S cm^{-1}]
PUTP1	10:1	−62.7	3.8×10^{-3}
PUTP2	5:1	−62.2	2.8×10^{-3}
PUTP3	2.5:1	−61.6	2.5×10^{-3}

The scanning electron microscopy (SEM) observations show a uniform and flat surface of PUTP solid electrolyte. The SEM images of PUTP1, PUTP2, and PUTP3 samples are shown in Figure 2d–f. This interface ensured good contact between the electrolyte and positive/negative electrodes in the cell. As shown in Figures S8–S10 (Supporting Information), the detailed elemental distribution scanning (EDS) results present the uniform distribution of C, N, O, F, and S elements, indicating a uniform distribution of LiTFSI in the PUTP electrolyte.

2.2. Physical Properties of Electrolytes

The thermal stability of PSEs is of vital importance to the safety of lithium metal batteries. Thermal gravimetric analysis (TGA) was conducted on three obtained electrolyte samples to investigate the effect of UPyMA on the thermal decomposition temperature. As shown in **Figure 3**a, the thermal decomposition curves of PUTP1, PUTP2, and PUTP3 showed their decomposition temperatures at 192, 270, and 270 °C, respectively. The decomposition temperatures of all polymer electrolytes are higher than the melting point of lithium metal (180 °C), confidently proving that these electrolytes can perform their duty safely in lithium metal batteries with qualified thermal stability.

The differential scanning calorimetry (DSC) results (Figure 3b) reveal T_g values as −62.7, −62.2, and −61.6 °C for PUTP1, PUTP2, and PUTP3 electrolytes, respectively. Furthermore, the T_g of PUTP1, PUTP2, and PUTP3 electrolytes have been found to increase with the increase of UPyMA content. The crystalline properties of three samples were examined by X-ray diffraction (XRD). There are no significant crystalline peaks from the XRD curves (Figure 3c), suggesting that all three polymeric solid electrolytes are in an amorphous form. The tensile testing results in Figure 3d demonstrate that, as UPyMA content increases, the maximum tensile strains of PUTP1, PUTP2, and PUTP3 electrolytes gradually increase, with PUTP3 having superior mechanical tensile properties with 48% maximum tensile strain. Apart from the chemical cross-linking, the physical cross-linking induced by the quadruple hydrogen bonding of UpyMA dimer also contributes to the mechanical enhancement of electrolytes.

2.3. Electrochemical Performance

In addition to the mechanical properties, the polymer electrolyte needs to reach several electrochemical merits to achieve a quality charging and discharging performance. The ionic conductivity, decomposition voltage, and lithium-ion transference number are three top electrochemical parameters for PSEs. First, AC impedance spectra were used to characterize the ionic conductivity of PUTP1, PUTP2, and PUTP3 (Figures S11–S13, Supporting Information). The ionic conductivity of three electrolytes (**Figure 4**a) is calculated by Equation (1) as a function of temperature from 25 to 70 °C. The ionic conductivity gradually increases when temperature elevates, it is found that the ionic conductivity with

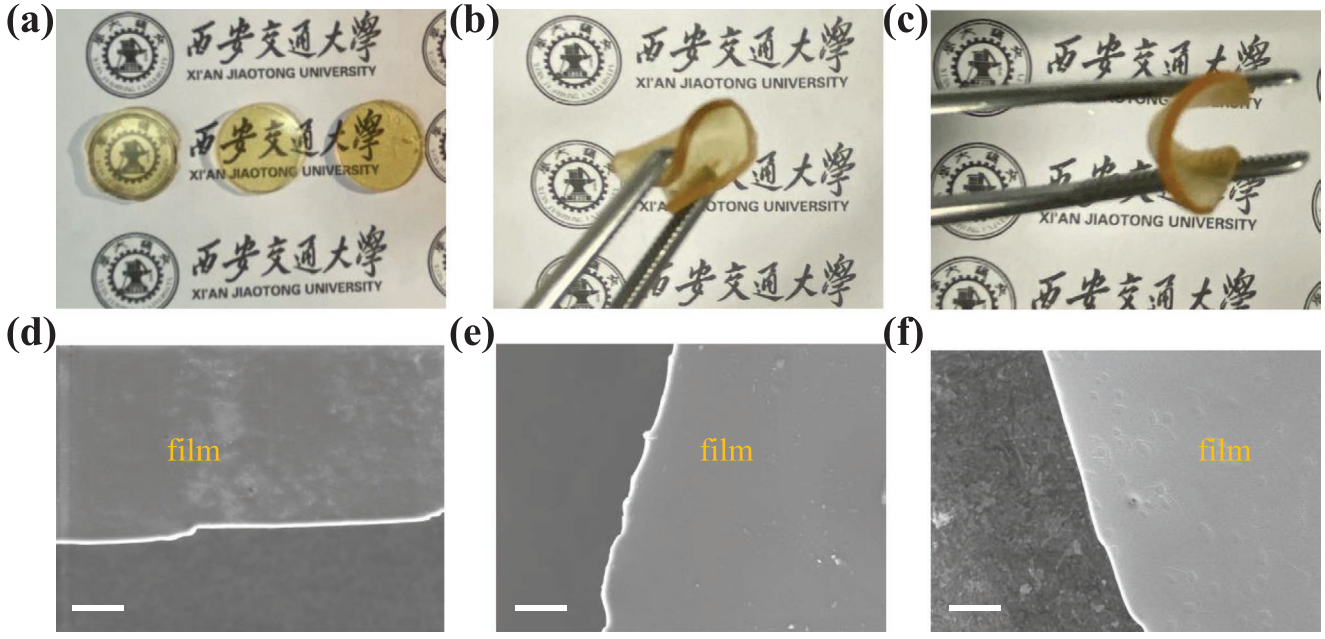

Figure 2. a) Optical images (from left to right) of PUTP1, PUTP2, and PUTP3. b) Photograph of PUTP1 electrolyte folded from the front with tweezers. c) Photograph of PUTP1 electrolyte folded from the back with tweezers. Scanning electron micrographs of d) PUTP1, e) PUTP2, and f) PUTP3. Scale bars: 20 µm.

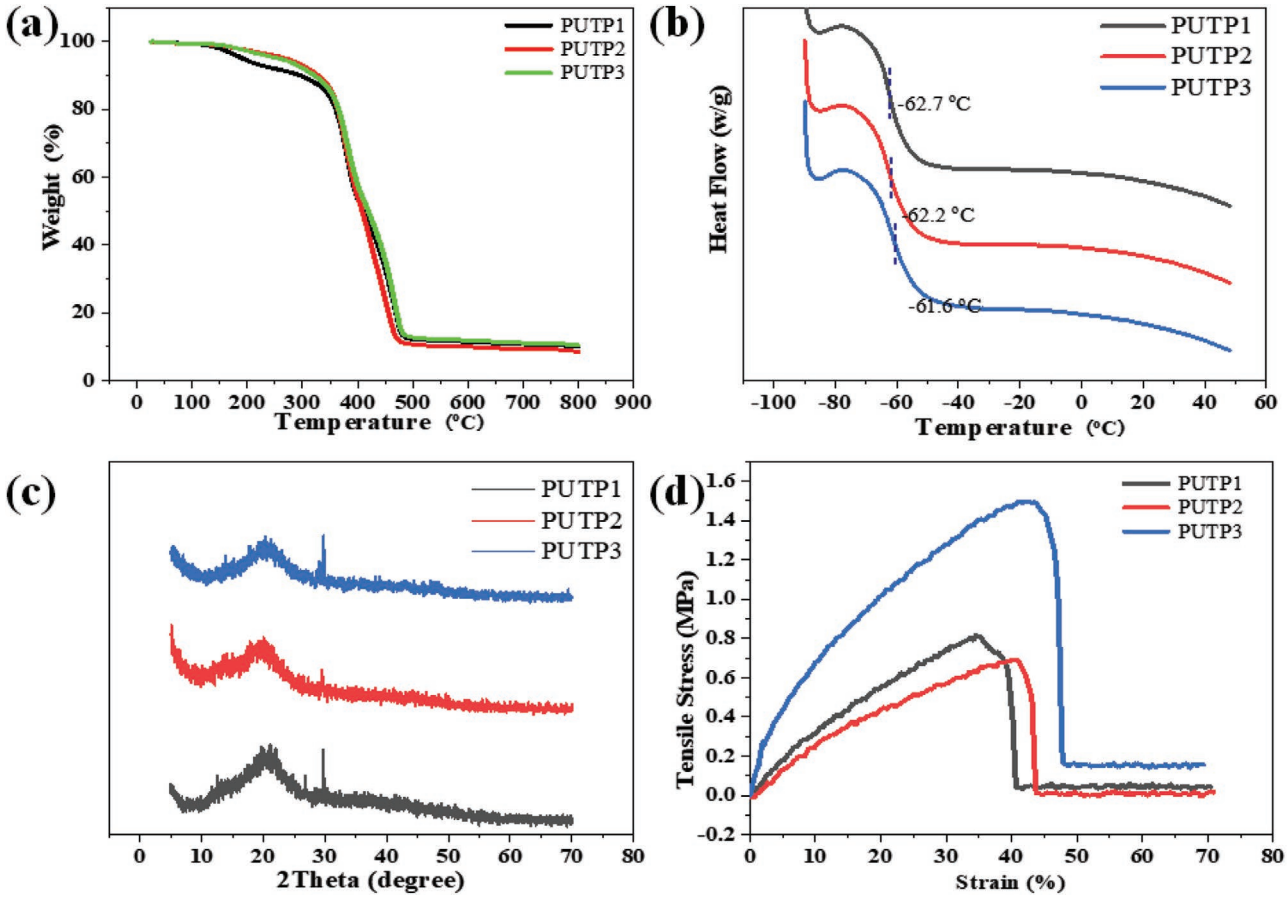

Figure 3. a) TGA curves of PUTP1, PUTP2, and PUTP3 performed under inert N_2. b) DSC curves of PUTP1, PUTP2, and PUTP3 were performed at −90–50 °C. c) XRD curves of PUTP1, PUTP2, and PUTP3 were conducted at 5–70. d) The stress–strain curve of PUTP1, PUTP2, and PUTP3, for which the parameters of the process in the test were set to a tensile rate of 10 mm min^{-1} and a sample size of $20 \times 5 \times 0.2$ mm^3.

temperature conforms to the Vogel–Tamman–Fulcher equation by fitting the conductivity curve. It is found that PUTP1 has the highest ionic conductivity of 3.8×10^{-3} S cm^{-1} at 25 °C. The ionic conductivity of PUTP2 and PUTP3 are 2.8×10^{-3} and 2.5×10^{-3} S cm^{-1} at 25 °C, respectively.

The electrochemical stability of polymer electrolyte is particularly important from the operational safety perspective, which requires the electrolyte not to decompose or undergo electrochemical reactions within the battery charging and discharging voltage range. The anodic limiting potentials of PUTP1, PUTP2, and PUTP3 were measured by linear scanning voltammetry (LSV) for Li/PUTP/stainless cells at 25 °C with LSV measurements in the voltage range 2.5–6 V versus Li/Li^+ at a scan rate of 1 mV s^{-1}. In Figure 4b, the LSV curves show a steady current plateau until 4.6 V, suggesting a high decomposition voltage above 4.6 V for all solid electrolytes. When the voltage exceeds 4.6 V, the current increases, indicating that the electrolyte starts to decompose. The wide electrochemical stability shows excellent electrochemical stability that could satisfy the requirements for a high voltage battery. As shown in Figure 4c, the calculated t_{Li+} (calculated by the Bruce–Vincent equation, Equation (2) for PUTP1, PUTP2, and PUTP3 are 0.13, 0.12, and 0.17, respectively. The low Li-ion transference number is caused by the existence of a significant number of freely flowing TFSI negative ions and mobile $AMIM^+$ cations in the electrolyte system. The constant potential polarization curves and AC impedance spectra of PUTP2 and PUTP3 are shown in Figures S14 and S15 (Supporting Information).

2.4. Battery Performance

The battery performance of obtained GPEs are measured at room temperature and 25 °C. As shown in Figure S16 (Supporting Information), the PUTP1 electrolyte exhibits a small overpotential in the Li/PUTP1/Li symmetric cell with an overpotential of 30 mV at a current density of 0.05 mA cm^{-2} and 75 mV at a current density of 0.1 mA cm^{-2}. The overpotential of the symmetric cell at cycling at different current densities showed an increase in voltage polarization along with the increment in current density. Interestingly, the overpotential remained approximately stable at the same current density, indicating that the electrolyte has good compatibility with lithium metal.[15] Moreover, the symmetric cells do not show a short circuit after cycling for 400 h, indicating a strong reliability. The Li/PUTP2/Li symmetric cell and the Li/PUTP3/Li symmetric cell both have a small overpotential and no short circuit after cycling (Figures S17 and S18, Supporting Information).

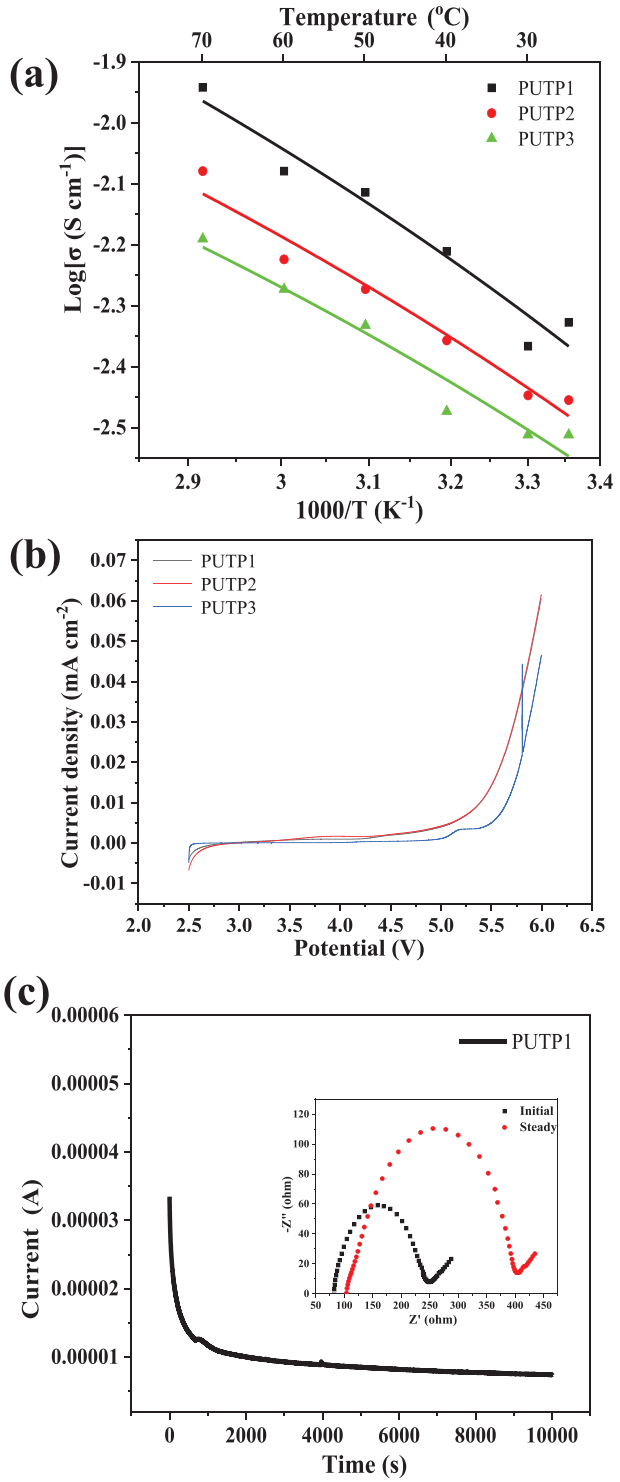

Figure 4. a) Temperature-dependent ionic conductivity of PUTP1, PUTP2, and PUTP3 thin-film electrolytes. b) LSV curves of PUTP1, PUTP2, and PUTP3 thin-film electrolytes. c) Chronoamperometry profile of Li/PUTP1/Li cells at 25 °C and the inset shows the impedance spectra before and after chronoamperometry.

The cyclic voltammetry curve of Li/PUTP1/LFP cell is shown in Figure S19 (Supporting Information), with 10 cycles in the voltage range of 2.5–4 V and a scan rate of 0.1 mV s^{-1}. The oxidation peak at 3.69 V represents the process of lithium-ion detachment from LFP, while the reduction peak at 3.17 V represents the process of lithium-ion embedding into LFP. After the first cycle is completed, the pair of redox peaks remains essentially unchanged, suggesting significant stability between the LFP cathode and the PUTP electrolyte. Additionally, the cyclic voltammetry curves of the Li/PUTP2/LFP cell and the Li/PUTP3/LFP cell are shown in Figures S20 and S21 (Supporting Information).

The charge/discharge voltage curves of the Li/PUTP1/LFP battery at 0.1C at a room temperature are clearly shown in **Figure 5**a, with the charge plateau at 3.49 V and the discharge plateau at 3.38 V. The difference value in charge and discharge voltage plateaus is 110 mV, which is compatible with asymmetric battery's lower polarization voltage. The charging and discharging plateaus are symmetrical, meaning that the electrochemical reactions that occur while charging and discharging in the cell are reversible.[16] In addition, Figure 5b shows that the lithium battery based on PUTP1 electrolyte can be better charged and discharged for at least 100 cycles at room temperature at 0.1C, and the Coulomb efficiency can reach more than 96%, and the initial discharge specific capacity of the battery is 155.6 mAh g^{-1}, and the discharge specific capacity remains at 126.2 mAh g^{-1} after 100 cycles, with a capacity retention rate of 81.1%.

The rate performance of the Li/PUTP1/LFP battery is shown in Figure 5c. The discharge specific capacity of battery at rate of 0.1C, 0.2C, 0.5C, 1C, 2C, and 0.1C are 133.4, 129.3, 119.8, 103.7, 69.0, and 131.4 mAh g^{-1}, respectively. The results of cell rate tests show that the PUTP1 electrolyte has a good rate performance. Li/PUTP2/LFP and Li/PUTP3/LFP cells rate performance are shown in (Figures S22 and S23, Supporting Information). Compared to PUTP1, PUTP2, and PUTP3 exhibit poor rate performance. Even though UPyMA can enhance the mechanical properties of electrolyte through quadruple hydrogen bonding, the rate capability performance deteriorates with increasing UPyMA. The three supramolecular gel polymer electrolytes PUTP1, PUTP2, and PUTP3 have a progressive increase in the proportion of UPyMA monomers, which increases the likelihood that UPyMA will be present on the surface of the electrolyte in higher amounts. Excessive UPyMA on the surface may lead to poor wettability between electrolyte and electrode, resulting in differences in rate capability. Figure 5d shows the charge/discharge cycling performance of the PUTP1 electrolyte at 0.2C at 25 °C. The Li/PUTP1/LFP coin cell was first assembled and activated by five charge/discharge cycles at 0.1C, followed by 60 cycles at 0.2C with an initial discharge specific capacity of 149.3 mAh g^{-1}. After 60 cycles, the specific capacity decays at a rate of 0.71 mAh g^{-1} per cycle, but still maintains a specific capacity of 106.4 mAh g^{-1}. In the supporting material, the charge/discharge cycles of a Li/PUTP2/LFP coin cell and a Li/PUTP3/LFP coin cell with 0.2C are shown (Figures S24 and S25, Supporting Information). The specific capacity of Li/PUTP3/LFP at 0.2C decays from 101.1 mAh g^{-1} at the beginning to 48.0 mAh g^{-1} after 60 cycles, which may be attributed to the increase in UPyMA content, which makes the electrolyte more likely to form dimers under prolonged operating conditions.

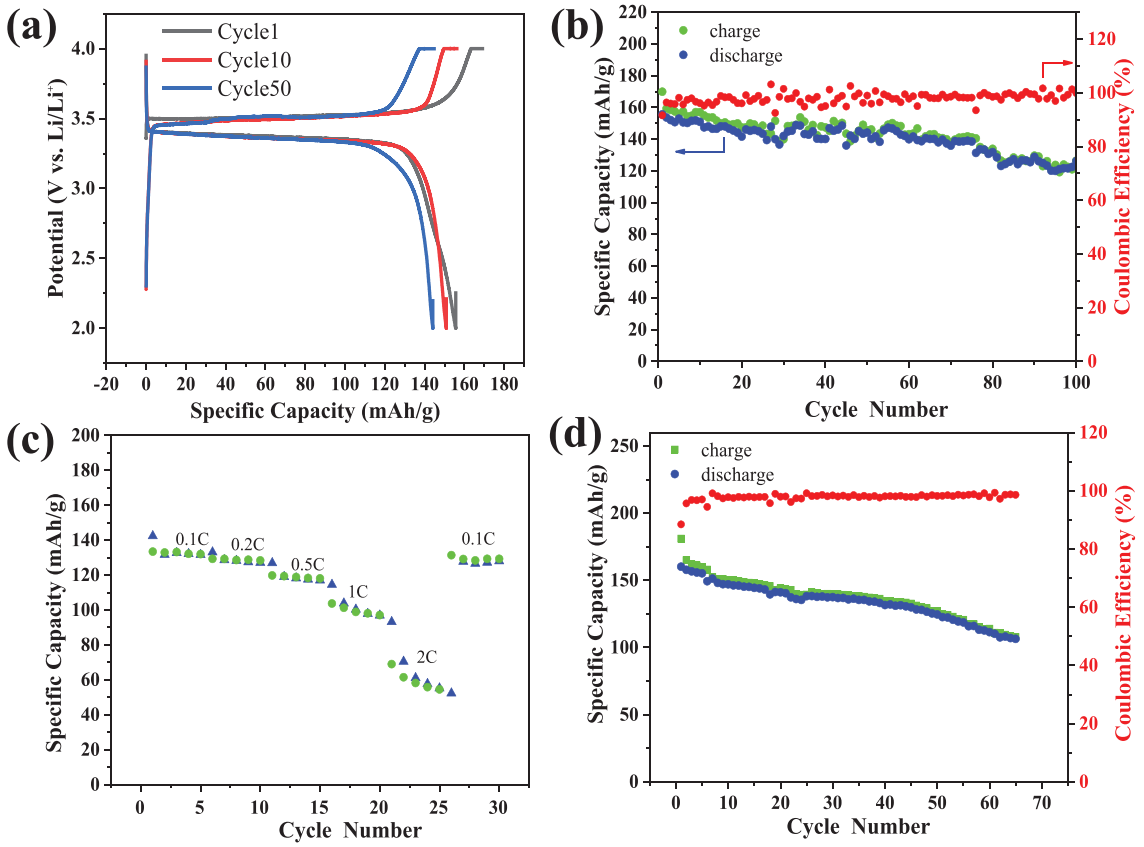

Figure 5. a) Voltage curves of Li/PUTP1/LFP battery charged and discharged at a current rate of 0.1 C at room temperature for the first, tenth and fiftieth cycles. b) Galvanostatic charge–discharge profiles of Li/PUTP1/LFP for 100 cycles at 0.1 C at room temperature. c) The rate capability of Li/PUTP1/LFP cell at 25 °C. d) Graphs of specific capacity and Coulombic efficiency at 0.2 C at 25 °C of PUTP1 base battery.

3. Conclusion

In summary, we describe a facile one-step UV light polymerization strategy to achieve supramolecular network GPEs. The mechanical properties of synthesized solid electrolytes are improved with the increase of UPyMA content (stretching rate ≈48% for PUTP3), while PUTP1 shows the highest ionic conductivity at 25 °C (3.8×10^{-3} S cm^{-1}). In addition, the GPEs in this paper not only have good mechanical strength but also possess high ionic conductivity. High ionic conductivity of GPEs is attributed to the ion transport by multiple ion channels in the supramolecular network structure, while the good mechanical properties of GPEs is due to the supramolecular network structure of UPyMA dimer. After assembling the solid-state electrolyte into a symmetric Li/PUTP/Li battery, it is found that the solid-state electrolyte has a small polarization voltage in the symmetric cell. The Li/PUTP1/LFP solid-state battery at 0.1C can not only achieve charge/discharge cycles at room temperature but also exhibits a better rate performance. This GPEs technique is expected to provide an opportunity for developing lithium metal batteries of high energy density and safe performance.

4. Experimental Section

Materials: Poly(ethylene glycol) methyl ether methacrylate (PEGMA, M_n = 500 g mol^{-1}, 98%, Aladdin), tripropylene glycol diacrylate (TPGDA, 99%, Aladdin), 1-Allyl-3-methylimidazolium Bis(trifluoromethanesulfonyl)imide (AMIMTFSI, 98%, TCI), 2-hydroxy-2-methylpropiophenone (97%, Aladdin), Bis(trifluoromethane)sulfonimide lithium salt (LiTFSI, >99%, Canrd), $LiFePO_4$ (LFP, battery degree, Canrd), *N*-methyl-2-pyrrolidone (NMP) are analytically pure obtained by Sinopharm Chemical Reagent Co., Ltd.

Synthesis of UPyMA: UPyMA was synthesized using steps from the literature, with some modifications to the literature synthesis.[14] 6-methylisocytosine (10 g, 80 mmol), 2-isocyanatoethyl methacrylate (13.2 g, 85 mmol), and 150 mL dimethyl sulfoxide (DMSO) solvent were added to a 250 mL two mouth flask and heated to 150 °C until a pale yellow solution was formed. To acquire UPyMA monomer, the solution is allowed to stand for 12 h before being filtered, rinsed three times with ethanol (50 mL), and dried at room temperature. The chemical reaction equation is shown in the diagram (Scheme S1, Supporting Information). The NMR hydrogen spectra showed that the UPyMA monomer was successfully prepared (Figure S26, Supporting Information).

Synthesis of PUTP Electrolyte: The polymer electrolyte was prepared by a facile one-step photopolymerization. Taking PUTP1 as an example, UPyMA (0.084 g, 0.3 mmol), TPGDA (0.18 g, 0.6 mmol), PEGMA (1.5 g, 3 mmol), AMIMTFSI (1.5 g, 1 mol kg^{-1} LiTFSI solution), LiTFSI (0.407 g, with the EO/Li^+ molar ratio of 16:1) and 2-hydroxy-2-methylpropiophenone (60 mg, 2 wt%) were dissolved in 4 mL DMSO. Then heated to 80 °C until the solution was completely clear and homogeneous. The above solution was then transferred to a Teflon mold and exposed to a UV light for 2 h at a wavelength of 365 nm. Finally, the polymer film dried under vacuum overnight at 80 °C/–0.09 MPa and denoted as PUTP1. The samples of PUTP2 and PUTP3 were synthesized similar to PUTP1, and the ratio of UPyMA to PEGMA is in Table 1. All samples were kept in the glove box (O_2 < 0.1 ppm, H_2O < 0.1 ppm) before testing.

The Ionic Conductivity Study: The ionic conductivity was measured in the frequency range of 100–10^6 Hz by electrochemical impedance spectroscopy (EIS) with a potential static signal amplitude of 10 mV. The electrolyte was sandwiched between two stainless steel electrodes in a Swagelok cell, from 25 to 70 °C with an increment of 10 °C (Correst, China). The Swagelok cells assembled in the glove box (O_2 < 0.1 ppm, H_2O < 0.1 ppm) and the ionic conductivity σ can be evaluated by the following equation

$$\sigma = L/RS \quad (1)$$

where R, L, and S are the bulk resistance, thickness, and area of the solid-state electrolyte slice, respectively.

Electrochemical Stability Assessment: The electrochemical stability of the solid electrolyte was tested by the linear sweep voltammetry (LSV) technique. LSV was performed in the potential of 2.5–6 V versus Li^+/Li at 25 °C (scan rate 1 mV s^{-1}) using a stainless steel/electrolyte/Li coin cells (CR2016), Li-metal diameter 14 mm, PUTP diameter 18 mm.

Lithium-Ion Transference Number: The symmetric Li/PUTP/Li cells were assembled to determine Li^+ transference number (t_{Li+}) using electrochemical impedance spectroscopy and chronoamperometry at 25 °C. The t_{Li+} of electrolytes PUTP1, PUTP2, and PUTP3 were calculated by the Bruce–Vincent–Evans equation, a polarization voltage (ΔV) of 10 mV was applied to the symmetrical cells, I_0 and I_s are the initial and steady-state current, while R_0 and R_s are the interfacial resistances at the initial and steady state, respectively

$$t_{Li^+} = \frac{I_s}{I_0}\frac{\Delta V - I_0 R_0}{\Delta V - I_s R_s} \quad (2)$$

Symmetric Cell: Li/PUTP/Li symmetric cell with constant current density plating/stripping at 0.05 and 0.1 mA cm^{-2}, respectively, with a plating/stripping cycle time of 0.5 h. The diameter of the PUTP electrolyte is 18 mm and the diameter of the lithium metal is 8 mm.

Preparation of Cathode Material: By spreading the mixture of LFP, Super P, and poly(vinylidene fluoride) (initially dissolved in NMP) with a weight ratio of 8: 1: 1 onto an aluminum current collector the positive electrode was manufactured. Then dried at 60 °C at least 24 h under ambient atmospheric pressure. Electrode sheet LFP with a load of 1.2–1.3 mg cm^{-2}.

Li Battery Assembly: Coin cells (CR2016) were assembled with LFP cathode, Li metal anode, and the solid-state electrolyte slices in a glove box filled with argon. Under a potential range of 2.0–4.0 V, the galvanostatic charge–discharge cycling output was reported on a LAND battery test device (CT2001A, LANHE, China). The charge and discharge current rates were fixed to C/10 at room temperature or C/5 at 25 °C.

Supporting Information

Supporting Information is available from the Wiley Online Library or from the author.

Acknowledgements

This work was supported by the National Natural Science Foundation of China (No. 21803040), Young Talent Support Plan of Xi'an Jiaotong University and the Engineering and Physical Sciences Research Council (EPSRC) Grant Nos. EP/N007921 and EP/S032886.

Conflict of Interest

The authors declare no conflict of interest.

Data Availability Statement

The data that support the findings of this study are available in the supplementary material of this article.

Keywords

gel polymer electrolytes (GPEs), high-voltage electrolytes, ionic conductivity, lithium metal batteries, supramolecular networks

Received: October 19, 2021
Revised: December 13, 2021
Published online: January 20, 2022

[1] a) Z. Chen, P.-C. Hsu, J. Lopez, Y. Li, J. W. F. To, N. Liu, C. Wang, S. C. Andrews, J. Liu, Y. Cui, Z. Bao, *Nat. Energy* **2016**, *1*, 15009; b) Q. S. Wang, P. Ping, X. J. Zhao, G. Q. Chu, J. H. Sun, C. H. Chen, *J. Power Sources* **2012**, *208*, 210.

[2] a) Y. Xiao, Y. Wang, S.-H. Bo, J. C. Kim, L. J. Miara, G. Ceder, *Nat. Rev. Mater.* **2020**, *5*, 105; b) C. Wang, K. Fu, S. P. Kammampata, D. W. McOwen, A. J. Samson, L. Zhang, G. T. Hitz, A. M. Nolan, E. D. Wachsman, Y. Mo, V. Thangadurai, L. Hu, *Chem. Rev.* **2020**, *120*, 4257; c) T. Jiang, P. He, G. Wang, Y. Shen, C.-W. Nan, L.-Z. Fan, *Adv. Energy Mater.* **2020**, *10*, 1903376; d) Q. Zhao, X. Liu, S. Stalin, K. Khan, L. A. Archer, *Nat. Energy* **2019**, *4*, 365; e) J. Wan, J. Xie, X. Kong, Z. Liu, K. Liu, F. Shi, A. Pei, H. Chen, W. Chen, J. Chen, X. Zhang, L. Zong, J. Wang, L.-Q. Chen, J. Qin, Y. Cui, *Nat. Nanotechnol.* **2019**, *14*, 705; f) M. Ebadi, T. Eriksson, P. Mandal, L. T. Costa, C. M. Araujo, J. Mindemark, D. Brandell, *Macromolecules* **2020**, *53*, 764;

[3] D. Lin, Y. Liu, Y. Cui, *Nat. Nanotechnol.* **2017**, *12*, 194.

[4] a) F. Guo, C. Wu, H. Chen, F. Zhong, X. Ai, H. Yang, J. Qian, *Energy Storage Mater.* **2020**, *24*, 635; b) B. Li, Y. Wang, S. Yang, *Adv. Energy Mater.* **2018**, *8*, 1702296; c) X. Yang, J. Luo, X. Sun, *Chem. Soc. Rev.* **2020**, *49*, 2140; d) H. Liu, X.-B. Cheng, J.-Q. Huang, H. Yuan, Y. Lu, C. Yan, G.-L. Zhu, R. Xu, C.-Z. Zhao, L.-P. Hou, C. He, S. Kaskel, Q. Zhang, *ACS Energy Lett.* **2020**, *5*, 833; e) H. Zhang, G. Gebresilassie Eshetu, X. Judez, C. Li, L. M. Rodriguez-Martinez, M. Armand, *Angew. Chem., Int. Ed.* **2018**, *57*, 15002; f) Z. Li, J. Huang, B. Y. Liaw, V. Metzler, J. Zhang, *J. Power Sources* **2014**, *254*, 168; g) D. Wang, W. Zhang, W. Zheng, X. Cui, T. Rojo, Q. Zhang, *Adv. Sci.* **2017**, *4*, 1600168.

[5] a) V. Bocharova, A. P. Sokolov, *Macromolecules* **2020**, *53*, 4141; b) K. Wu, J. Huang, J. Yi, X. Liu, Y. Liu, Y. Wang, J. Zhang, Y. Xia, *Adv. Energy Mater.* **2020**, *10*, 1903977; c) D. Zhou, D. Shanmukaraj, A. Tkacheva, M. Armand, G. Wang, *Chem* **2019**, *5*, 2326; d) K. S. Ngai, S. Ramesh, K. Ramesh, J. C. Juan, *Ionics* **2016**, *22*, 1259.

[6] a) W. Liu, S. W. Lee, D. Lin, F. Shi, S. Wang, A. D. Sendek, Y. Cui, *Nat. Energy* **2017**, *2*, 17035; b) I. Osada, H. de Vries, B. Scrosati, S. Passerini, *Angew. Chem., Int. Ed.* **2016**, *55*, 500; c) L. Long, S. Wang, M. Xiao, Y. Meng, *J. Mater. Chem. A* **2016**, *4*, 10038.

[7] a) Y. Li, Z. Sun, L. Shi, S. Lu, Z. Sun, Y. Shi, H. Wu, Y. Zhang, S. Ding, *Chem. Eng. J.* **2019**, *375*, 121925; b) C. Wang, T. Wang, L. Wang, Z. Hu, Z. Cui, J. Li, S. Dong, X. Zhou, G. Cui, *Adv. Sci.* **2019**, *6*, 1901036.

[8] G. Wang, X. Zhu, A. Rashid, Z. Hu, P. Sun, Q. Zhang, L. Zhang, *J. Mater. Chem. A* **2020**, *8*, 13351.

[9] Z. P. Wan, D. N. Lei, W. Yang, C. Liu, K. Shi, X. G. Hao, L. Shen, W. Lv, B. H. Li, Q. H. Yang, F. Y. Kang, Y. B. He, *Adv. Funct. Mater.* **2019**, *29*, 1805301.

[10] R. Bouchet, S. Maria, R. Meziane, A. Aboulaich, L. Lienafa, J. P. Bonnet, T. N. Phan, D. Bertin, D. Gigmes, D. Devaux, R. Denoyel, M. Armand, *Nat. Mater.* **2013**, *12*, 452.

[11] a) C. Cao, Y. Li, Y. Feng, P. Long, H. An, C. Qin, J. Han, S. Li, W. Feng, *J. Mater. Chem. A* **2017**, *5*, 22519; b) C. Cao, Y. Li, S. Chen, C. Peng, Z. Li, L. Tang, Y. Feng, W. Feng, *ACS Appl. Mater. Interfaces* **2019**, *11*, 35683; c) C. Cao, Y. Li, Y. Feng, C. Peng, Z. Li, W. Feng, *Energy Storage Mater.* **2019**, *19*, 401.

[12] B. Zhou, M. Yang, C. Zuo, G. Chen, D. He, X. Zhou, C. Liu, X. Xie, Z. Xue, *ACS Macro Lett.* **2020**, *9*, 525.

[13] a) J. Hu, W. Wang, B. Zhou, Y. Feng, X. Xie, Z. Xue, *J. Membr. Sci.* **2019**, *575*, 200; b) G. Jo, H. Jeon, M. J. Park, *ACS Macro Lett.* **2015**, *4*, 225; c) H. Duan, Y.-X. Yin, X.-X. Zeng, J.-Y. Li, J.-L. Shi, Y. Shi, R. Wen, Y.-G. Guo, L.-J. Wan, *Energy Storage Mater.* **2018**, *10*, 85; d) W. Fan, N.-W. Li, X. Zhang, S. Zhao, R. Cao, Y. Yin, Y. Xing, J. Wang, Y.-G. Guo, C. Li, *Adv. Sci.* **2018**, *5*, 1800559.

[14] B. Zhou, D. He, J. Hu, Y. Ye, H. Peng, X. Zhou, X. Xie, Z. Xue, *J. Mater. Chem. A* **2018**, *6*, 11725.

[15] T. Dong, J. Zhang, G. Xu, J. Chai, H. Du, L. Wang, H. Wen, X. Zang, A. Du, Q. Jia, X. Zhou, G. Cui, *Energy Environ. Sci.* **2018**, *11*, 1197.

[16] X. Tian, P. Yang, Y. Yi, P. Liu, T. Wang, C. Shu, L. Qu, W. Tang, Y. Zhang, M. Li, B. Yang, *J. Power Sources* **2020**, *450*, 227629.